Nonlocal Impacts of Soil Moisture Variability in South America: Linking Two Land–Atmosphere Coupling Hot Spots

JULIÁN ALBERTO GILES,[a,b,c] CLAUDIO GUILLERMO MENÉNDEZ,[b,c,d] AND ROMINA CARLA RUSCICA[a,b,c]

[a] *Universidad de Buenos Aires, Facultad de Ciencias Exactas y Naturales, Buenos Aires, Argentina*
[b] *CONICET–Universidad de Buenos Aires, Centro de Investigaciones del Mar y la Atmósfera (CIMA), Buenos Aires, Argentina*
[c] *CNRS–IRD–CONICET–UBA, Instituto Franco-Argentino para el Estudio del Clima y sus Impactos (IRL 3351 IFAECI), Buenos Aires, Argentina*
[d] *Universidad de Buenos Aires, Facultad de Ciencias Exactas y Naturales, Departamento de Ciencias de la Atmósfera y los Océanos, Buenos Aires, Argentina*

(Manuscript received 2 July 2021, in final form 1 September 2022)

ABSTRACT: The land–atmosphere interactions play an important role in modulating climate variability at different spatial and temporal scales. In South America, two recognized hot spots of soil moisture–atmosphere coupling are located in southeastern South America (SESA) and eastern Brazil. Soil moisture variability may not only alter the climate locally but may also have nonlocal impacts through changes in the regional circulation. Here we explore how these two local coupling hot spots interact with each other, how soil moisture variability modulates the regional circulation, and what is the consequent nonlocal impact on precipitation. To this end, we analyze numerical experiments, performed with a regional climate model for the period October–March of 1983–2012, that allow us to isolate the influence of the soil moisture interannual variability on the regional climate. When the soil moisture–atmosphere interaction is enabled, we find a nonlocal coupling mechanism that links both hot spots at different temporal scales, favoring precipitation in eastern Brazil to the detriment of the precipitation in SESA through shifts in the regional circulation, when compared with a simulation with constrained soil moisture–atmosphere interaction. In northeastern Argentina, a subregion of SESA located at the exit of the South American low-level jet, it was found that the amount of nighttime precipitation is modulated by the proposed nonlocal coupling mechanism. A better understanding of the variability of precipitation due to the influence of land–atmosphere interaction processes may contribute to improving the predictability of precipitation and the interpretation of climate projections.

KEYWORDS: South America; Atmosphere–land interaction; Climate variability; Soil moisture; Numerical analysis/modeling; Regional models

1. Introduction

Land–atmosphere interactions play an important role in modulating the climate variability at different spatial and temporal scales (Seneviratne et al. 2010), particularly, the variability of soil moisture (SM) can affect atmospheric processes, especially in transitional climate regions (Koster et al. 2004). In South America, two main hot spots of land–atmosphere coupling in southeastern South America (SESA) and eastern Brazil have been widely identified in previous works (Sörensson and Menéndez 2011; Wei and Dirmeyer 2012; Ruscica et al. 2015, 2016; Spennemann et al. 2018; Menéndez et al. 2016, 2019; Baker et al. 2021). Since the coupling hot spots coincide with important agricultural areas of Argentina, Brazil, Paraguay, and Uruguay, the ability of the SM variations to modulate the interannual variations of the regional climate may have consequences on the macroeconomics of these countries (Lachaud et al. 2017; Banerjee et al. 2021). However, the land–atmosphere coupling in these two hot spots has usually been studied on a local scale, not considering the hot spots as interacting regions, even though nonlocal influences have occasionally been suggested (Grimm et al. 2007; Bieri et al. 2021). Strong local SM–temperature coupling has been reported in South America, especially during austral spring and summer (Menéndez et al. 2019), as well as its influence on extremes (Coronato et al. 2020), whereas the local SM–precipitation coupling signal has been found to be usually weak or not significant (Sörensson and Menéndez 2011; Ruscica et al. 2015; Giles et al. 2021).

SM anomalies can influence the local input of moisture to the atmosphere (Eltahir and Bras 1996) and the energy balance and development of the boundary layer (Ek and Holtslag 2004). However, the effect on climate may not be limited to the region experiencing the SM anomalies but could affect other regions through the modification of the thermodynamic properties of the air, such as its humidity content, which is advected by regional or large-scale circulation, without necessarily implying changes in circulation patterns (e.g., Rowntree and Bolton 1983). Wei and Dirmeyer (2019) found globally that boreal summer precipitation P is more sensitive to local than nonlocal evapotranspiration E for most land areas, but some regions are sensitive to E from more than 1000 km away. Remote sensitivities are usually weaker than local ones, but their combined effect could be large. Another possible nonlocal effect of SM is through its impact on the temperature and pressure horizontal gradients and consequently on circulation, particularly during dry periods (Pal and Eltahir 2003; Fischer et al. 2007; Haarsma et al. 2009). Studies

Corresponding author: Julián Alberto Giles, julian.giles@cima.fcen.uba.ar

DOI: 10.1175/JCLI-D-21-0510.1

around the globe have found evidence of SM anomalies altering regional circulation patterns, which affects the surface air temperature and/or P of distant areas (e.g., Kanamitsu and Mo 2003; Vautard et al. 2007; Koster et al. 2014, 2016); however, the understanding of these nonlocal mechanisms is still insufficient (Seneviratne et al. 2010; Wei and Dirmeyer 2019), motivating our study.

In South America, the South American monsoon system and the large-scale leading modes of climate variability drive the characteristics of the atmospheric circulation, P, and surface air temperature over the continent, with ENSO as the main source of interannual variability (Garreaud et al. 2009; Marengo et al. 2012; Kayano et al. 2017; Montini et al. 2019). Another important source of variability at the interannual and intraseasonal scales is the dipole-like spatial pattern between SESA and the South Atlantic convergence zone, which develops during the warm season. This pattern is related to circulation changes that promote opposing P anomalies between those two regions (Nogués-Paegle and Mo 1997; Grimm and Zilli 2009; Junquas et al. 2012). In particular, SESA is affected by the moisture and energy transported by the South American low-level jet (SALLJ), especially by Chaco jet events (Salio et al. 2002; Marengo et al. 2004; Saulo et al. 2007). These intense SALLJ events bring moisture to central Argentina and are usually also related to the intrusion of a cold front from the south (Salio et al. 2007), favoring the development of mesoscale systems in the Andes foothills that then travel east, precipitating mostly at night (Velasco and Fritsch 1987; Romatschke and Houze 2010; Lavin-Gullon et al. 2021). These intense P systems pose a threat to the low-lying areas of the region that are prone to suffer recurrent floods, which are exacerbated because of the increasing land use changes, amplifying risks and social vulnerabilities (Murgida et al. 2014; Barros et al. 2015).

Some efforts to link the land surface influence on South American atmospheric circulation and P have been made over particular regions. In one study, Saulo et al. (2010) found that dry SM anomalies in northwestern Argentina resulted in stronger flow from tropical latitudes through the SALLJ into the northwestern Argentina low region, and similar results linked to Chaco jet events were found recently by Yang and Dominguez (2019). Grimm et al. (2007) found a regional mechanism at the seasonal scale in which dry soil conditions in eastern Brazil generate a cyclonic anomaly and draw moisture into that region and away from the SALLJ region, where the winds are weakened by an opposing northward anomaly. Evidence of the influence of dry SM anomalies in SESA on the regional circulation and P was also found recently by Bieri et al. (2021). In another study, Giles et al. (2021) analyzed rainy-night days in northeastern Argentina—at the exit of the SALLJ within the SESA coupling hot spot (hereinafter JEXIT)—and found an apparent contradiction: the comparison between climate simulations with and without SM–atmosphere interaction suggests that JEXIT rainy-night days are sensitive to the SM variability despite the local SM–atmosphere coupling being negligible during those days. Thus, they hypothesized that JEXIT rainy nights are affected by nonlocal effects of the land–atmosphere coupling (i.e., changes in the regional circulation product of the local land–atmosphere coupling in certain areas). This hypothesis, nonetheless, remains to be tested; it serves as motivation to further explore how the land–atmosphere interactions modulate the broad range of variabilities at the continental scale.

In this work we seek to analyze the local and nonlocal impacts of land–atmosphere coupling in South America. We hypothesize that the SM variability in coupling hot spots can alter temperature and pressure gradients at the continental scale, and thus alter the circulation patterns and horizontal moisture fluxes, eventually impacting the P in other regions. Using experiments carried out with the RCA4 regional climate model, we isolate the influence of the SM interannual variability on the climatology of South America, and particularly explore the influence on rainy-night events in JEXIT in order to test the hypothesis of Giles et al. (2021). The study of the JEXIT region aims at improving our understanding of the different conditions under which the local coupling is relevant and how it relates to the nonlocal coupling. We find links between two local land–atmosphere coupling hot spots and explore the relationship between interannual and diurnal variabilities.

2. Method and data

Using the SMHI Rossby Centre Regional Atmospheric Climate Model, version 4 (RCA4; SMHI 2021), we studied the land–atmosphere local and nonlocal coupling over most of the South American continent (0°–40°S, 70°–37°W), in the monsoon (wet) season (October–March) from 1983 to 2012. We analyzed the impacts on the long-term (30 yr) mean climate and during specific atmospheric conditions in JEXIT, looking at 12 modeled variables.

a. *RCA4 regional climate model and sensitivity experiments*

The RCA4 model was run over the whole South American continent and adjacent oceans at 0.5° × 0.5° resolution, driven by initial and boundary conditions from the ERA-Interim reanalysis (Dee et al. 2011). The version of RCA4 considered in this study is currently used within the context of the CORDEX project (http://www.cordex.org; Gutowski et al. 2016; Falco et al. 2019a; Feron et al. 2019; Solman and Blázquez 2019; Blázquez and Solman 2020) and has been widely analyzed over South America (Ruscica et al. 2015; Spennemann et al. 2018; Menéndez et al. 2016, 2019; Zaninelli et al. 2019; Giles et al. 2020, 2021; Coronato et al. 2020), and particularly over Argentina (Collazo et al. 2018; Giles et al. 2021). Table 1 provides a summary of the model configuration used in this study, including parameterizations and information of the land surface scheme.

Two 30-yr RCA4 simulations specifically designed for land surface–atmosphere coupling studies were used in this study, selecting the 1983–2012 period. They consist of a control run (CTL) and a second run in which the land surface is uncoupled from the atmosphere (UNC) by prescribing the SM of each time step with the corresponding CTL SM climate mean of the given day. Then, the CTL and UNC simulations have identical SM climate means, but in UNC the SM does not respond to either P or E. Hence, the UNC run eliminates

TABLE 1. Summary of the RCA4 model characteristics and the configurations used in the simulations.

	Configuration
Spatial domain	South America and adjacent oceans (CORDEX Region 1)
Projection	Rotated with north pole at 55°N, 70°W
Horizontal resolution	0.5° × 0.5°
Vertical coordinate/levels	Hybrid/40
Initial and lateral boundary conditions	6-h ERA-Interim reanalysis (Dee et al. 2011)
Time step	20 min
	Parameterizations
Advection scheme	Semi-Lagrangian, semi-implicit (Jones et al. 2004)
Radiation scheme	Savijärvi (1990), Sass et al. (1994); CO_2 absorption from Räisänen et al. (2000)
Convection scheme	Kain and Fritsch (1990, 1993) is used over South America instead of the Bechtold–"KF" scheme (Bechtold et al. 2001)
Cloud microphysics scheme	Rasch and Kristjánsson (1998)
	Land surface scheme (Samuelsson et al. 2015)
Land-use physiography	ECOCLIMAP (Masson et al. 2003)
Soil moisture/temperature layers	3 layers (first and second of constant depth; third variable according to root depth of ECOCLIMAP) / 5 layers
Vertical transport of water	Richards equation (Hillel 1980)
Soil texture	12 classes based on soil textural triangle (Hillel 1980) and the sand and clay content of soil (FAO-Unesco 1981)

all SM variabilities except for its climatological annual cycle. This is a commonly applied method in land–atmosphere coupling studies (Koster et al. 2000; Seneviratne et al. 2006; Conil et al. 2007; Krakauer et al. 2010; Jaeger and Seneviratne 2011; Hauser et al. 2017).

To illustrate the difference between simulations, Fig. 1 shows the interannual variability of top SM (7 cm) and E for each run, spatially averaged over JEXIT (25°–30°S and 62°–58°W; the outlined rectangle in Fig. 2). In CTL both variables have similar variability since JEXIT is mostly located within a transitional climate zone and changes in SM limit the water available for E, but in UNC the SM remains constant from year to year and is not affected by E or P. Then, by comparing CTL and UNC it is possible to isolate the influence that the SM interannual variability has on the atmosphere in order to study causality. This exact pair of simulations was analyzed in Menéndez et al. (2019) and Giles et al. (2021) and the reader can refer to those studies for a validation of P and 2-m temperature (T2m). The statistical significance of our results is tested

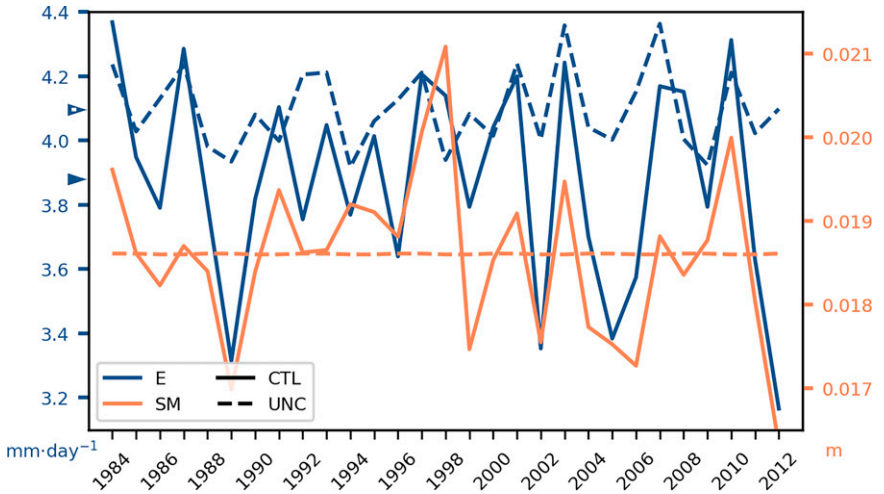

FIG. 1. Yearly mean top soil moisture (SM; right axis) and evapotranspiration (E; left axis) for CTL (solid) and UNC (dashed) simulations, averaged over JEXIT (rectangle in Fig. 2, below) during the monsoon (wet) season for 1983–2012. The labeled year corresponds to the year of the end of the season; for example, the value for 2005 represents the mean from October 2004 to March 2005. The climate means of E for both simulations are marked with triangles along the left axis; their difference is statistically significant at the 95% level according to Welch's t test.

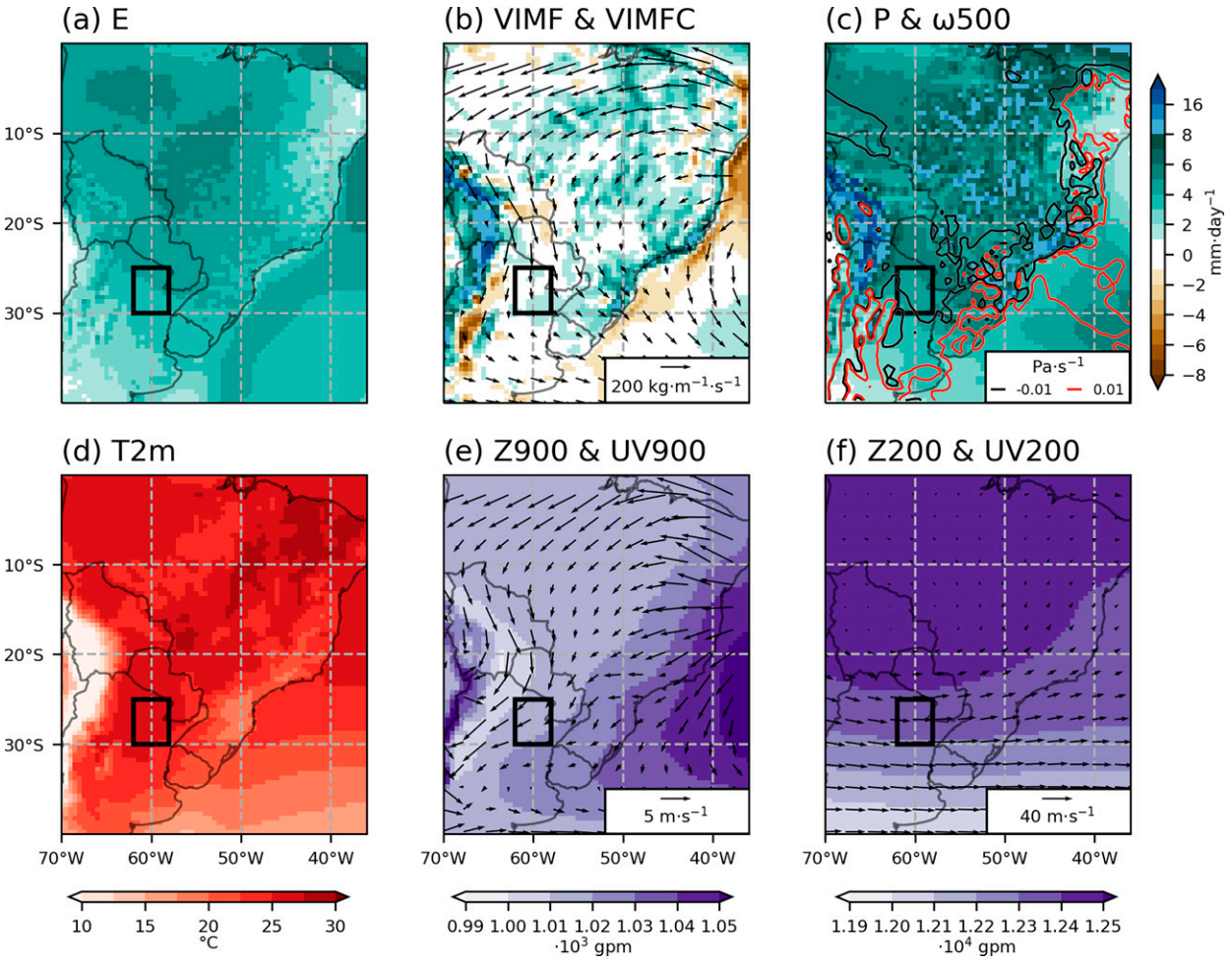

FIG. 2. Monsoon (wet) season 1983–2012 RCA4-CTL climate mean (a) evapotranspiration, (b) vertically integrated moisture flux and its convergence (positive values indicate convergence), (c) precipitation and 500-hPa omega vertical wind (positive values indicate subsidence), (d) 2-m temperature, (e) 900-hPa geopotential height and horizontal wind, and (f) 200-hPa geopotential height and horizontal wind. Fluxes and horizontal winds are represented by vectors, vertical wind is represented by contours, and all other variables are shown as shadings. The outlined rectangle indicates the JEXIT region.

with Student's t test or Welch's unequal variances t test (Welch 1947), clarified in each figure's caption.

Table 2 summarizes the acronyms or symbols of all RCA4 variables analyzed throughout this study; 10 of those (except LHF and SM) are analyzed at the continental scale in most of the figures.

b. *Atmospheric conditions in JEXIT*

In the JEXIT region we classified clear-sky, rainy-afternoon, and rainy-night days in the same way as in Giles et al. (2021), based on the works of Zhang and Klein (2010) and Tao et al. (2019). Using local solar time (LST = UTC − 4 h) and based on area-averaged hourly values of P and total and low cloud cover (TCC and LCC, respectively), we defined the following:

- *clear-sky days*: those with $P = 0$ during all hours and with TCC < 15% and LCC < 5% from 0800 to 1600 LST;
- *rainy-afternoon days*: those for which the maximum hourly P rate is located between 1200 and 2100 LST, it is greater than 1 mm day^{-1}, and it is at least 50% greater than the P rate outside the 1200–2100 LST range and the hourly P rate between 0000 and 1000 LST is lower than 1 mm day^{-1}; and
- *rainy-night days*: those for which the maximum hourly P rate is greater than 1 mm day^{-1} and is located between 0000 and 0600 LST.

Daily values were computed from midnight to midnight for clear-sky and rainy-afternoon days, and from 0900 LST of the previous day to 0900 LST of the event day for rainy-night days, so that the P event itself is located at the end of the 24-h period. For a validation of the modeled P events, the reader can refer to Giles et al. (2021). For a comparison of the mean diurnal cycle of P between RCA4 and other datasets, the reader can refer to Giles et al. (2020).

TABLE 2. List of acronyms and symbols for all variables mentioned throughout the study.

Variable	Description
E	Evapotranspiration (mm day^{-1})
T2m	2-m temperature (°C)
P	Precipitation (mm day^{-1})
ω500	Vertical wind at 500 hPa ($\omega > 0$ means subsidence, and vice versa) (Pa s^{-1})
VIMF	Vertically integrated moisture flux (kg m^{-1} s^{-1})
VIMFC	Vertically integrated moisture flux convergence (mm day^{-1})
Z900	Geopotential height at 900 hPa (gpm)
Z200	Geopotential height at 200 hPa (gpm)
UV900	Horizontal wind at 900 hPa (m s^{-1})
UV200	Horizontal wind at 200 hPa (m s^{-1})
SM	Soil moisture (m) (top 7-cm layer)
LHF	Latent heat flux (W m^{-2})

c. *Terrestrial coupling index*

To quantify the strength of the local SM–atmosphere coupling we calculated the Terrestrial Coupling Index (TCI; Dirmeyer 2011). This index uses the daily slope of the relationship between the SM and the latent heat flux (LHF), weighted by the SM standard deviation, to quantify how much the SM changes drive the surface heat flux variability. The TCI can be expressed in terms of the slope or the covariance between daily time series of SM and LHF in the following way:

$$\mathrm{TCI(SM, LHF)} = \mathrm{cov(SM, LHF)}/\sigma\mathrm{(SM)} = \rho\mathrm{(SM, LHF)} \times \sigma\mathrm{(SM)}, \quad (1)$$

where cov(SM, LHF) is the covariance between SM and LHF, σ(SM) is the standard deviation of SM, and ρ(SM, LHF) is the linear-regression slope between SM and LHF. A positive covariance (or ρ), and consequently a positive TCI, are indicative of land–atmosphere interaction since LHF depends directly on SM. The daily values used in the calculation are anomalies with respect to the monthly mean to avoid seasonal biases. The TCI was already used with RCA4 data in a comparison with satellite products (Spennemann et al. 2018), and it is different from other indices applied in the region (Sörensson and Menéndez 2011; Ruscica et al. 2016; Menéndez et al. 2019).

3. Results

a. *Mean climate*

First, the monsoon wet season climate reproduced by RCA4-CTL is presented in Fig. 2 through the mean fields of the variables described in Table 2. The E has its maximum in central Brazil and decreases toward eastern Brazil and central Argentina (Fig. 2a), following the water and energy availability at the surface (Seneviratne et al. 2010). The vertically integrated moisture flux (VIMF) pattern shows a primarily east–west direction from the equator up to 10°S, following the trade winds, and rotates anticlockwise farther south, intensifying along the Andes foothills (vectors in Fig. 2b). Most of Brazil shows positive vertically integrated moisture flux convergence (VIMFC) as well as over the Andes due to topographic effects, while divergence occurs along the Atlantic coast and over some spots close to the Andes slopes (shadings in Fig. 2b). The P reaches its maximum values in the Brazilian core monsoon region (shadings in Fig. 2c) and over the Andes. Areas with subsidence at middle levels of the troposphere are usually located over semiarid regions or over the ocean ($\omega500 > 0$; contours in Fig. 2c), while the monsoon region presents upward motion on average ($\omega500 < 0$ in Fig. 2c). T2m increases with decreasing latitude and with increasing distance from the Atlantic Ocean south of 20°S. The warmest temperatures are located in central and northeastern Brazil as well as around 20°S–55°W close to the Bolivia–Brazil–Paraguay triple border (Fig. 2d). At low tropospheric levels, the geopotential height (Z900) highlights the South Atlantic anticyclone and the northwestern Argentina and Chaco lows (shadings in Fig. 2e), and the winds (UV900) move westward from the equator up to 10°S, turning to the prevailing north–south direction along the Andes (vectors in Fig. 2e). At upper levels, we observe the westerlies south of 25°S and an anticyclonic gyre at low latitudes (UV200; vectors in Fig. 2f).

b. *Local land–atmosphere coupling (TCI)*

To explore whether and where the SM state can influence the local atmospheric conditions, Fig. 3 shows the TCI for all days in the period as well as for JEXIT clear-sky, rainy-afternoon, and rainy-night days, in CTL. In general, the TCI spatial patterns show, in positive values, the two land–atmosphere coupling hot spots in eastern Brazil and SESA, which are usually found in previous works. This was expected since the TCI is calculated from surface variables (i.e., SM and LHF) that are known to be related in climatic transition zones. In particular, JEXIT is located within the SESA hot spot. However, it is evident that the TCI changes depending on the atmospheric conditions: relative to the whole period (Fig. 3a), the TCI in and around JEXIT intensifies during JEXIT clear-sky days (Fig. 3b); it remains similar during rainy-afternoon days (Fig. 3c), and during rainy-night days it becomes negative (Fig. 3d), meaning that the SM does not influence the local state of the lower atmosphere. JEXIT rainy-night days are then not influenced by the local coupling, but the coupling can be relevant to other atmospheric conditions. Some changes in the TCI are also observed in other areas such as southern Brazil, Uruguay, and central Argentina.

c. *JEXIT rainy-night days: Average characteristics and forcings*

Since JEXIT rainy-night days are not influenced by the local land–atmosphere coupling, we will explore which are the regional atmospheric conditions associated with these events. As we mentioned in the introduction, SESA, and particularly JEXIT, is influenced by the continental transport of moisture and energy through the SALLJ, especially during nocturnal P events. Therefore, Fig. 4 shows the rainy-night days composite anomalies with respect to the mean climate (Fig. 2). Remember that we compare daily means and P peaks at night (by definition) but other variables (like E and T2m) maximize in

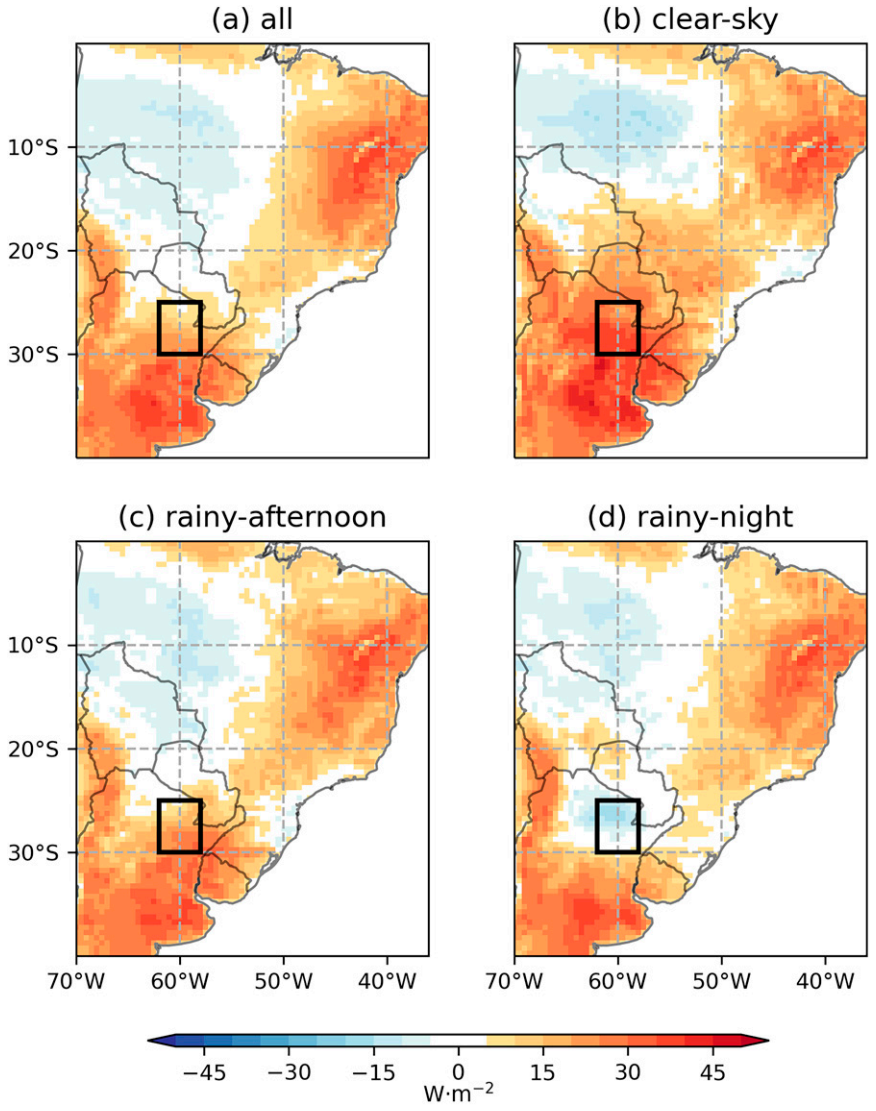

FIG. 3. Terrestrial coupling index (TCI) for (a) all days (all), (b) clear-sky days, (c) rainy-afternoon days, and (d) rainy-night days in JEXIT during the monsoon (wet) season for 1983–2012 in CTL. Only values that are statistically significant at the 95% level according to Student's *t* test are shown. The outlined rectangle indicates the JEXIT region.

the afternoon prior to the event (Giles et al. 2021). This means that the possible relationships between some variables, particularly between SM, *E*, and T2m, will be found in the hours previous to the peak in *P*.

JEXIT rainy-night days are characterized by intense *P* beyond JEXIT, from northern Argentina to Uruguay and southern Brazil, which is considerably higher than the climate mean (Fig. 4c). This is accompanied by an intensification of the Chaco low with respect to the mean climate (Z900 in Fig. 4e) as well as more intense low-level winds in the SALLJ area (Fig. 4e), which results in higher VIMF and VIMFC in the region (Fig. 4b). The *E* before the *P* event (since most *E* occurs during the day hours) shows a small increase relative to the climate mean from eastern Bolivia to central Argentina, Uruguay, and southern Brazil, while eastern Brazil and part of the Atlantic experience reduced *E* (Fig. 4a; *E* is multiplied by 10 to be comparable to the scale of changes in *P* and VIMFC). T2m increases from southern Bolivia to southern Brazil (Fig. 4d), coherently with the stronger northerly winds in low levels that carry warm moist air (Fig. 4e); also, central Argentina experiences colder T2m associated with southerly low-level winds (Fig. 4e). These anomalies in T2m and 900-hPa winds are consistent with the northeastward advance of a cold front, resulting in a strong baroclinic zone in JEXIT (Garreaud 2000). At upper levels, a wave train structure is observed (Fig. 4f), with centers of lower-higher-lower Z200 located from central Argentina to eastern Brazil. All in all, the pattern resembles that of a Chaco jet event, one type of manifestation of the SALLJ (Salio et al. 2002, 2007; Saulo et al. 2007).

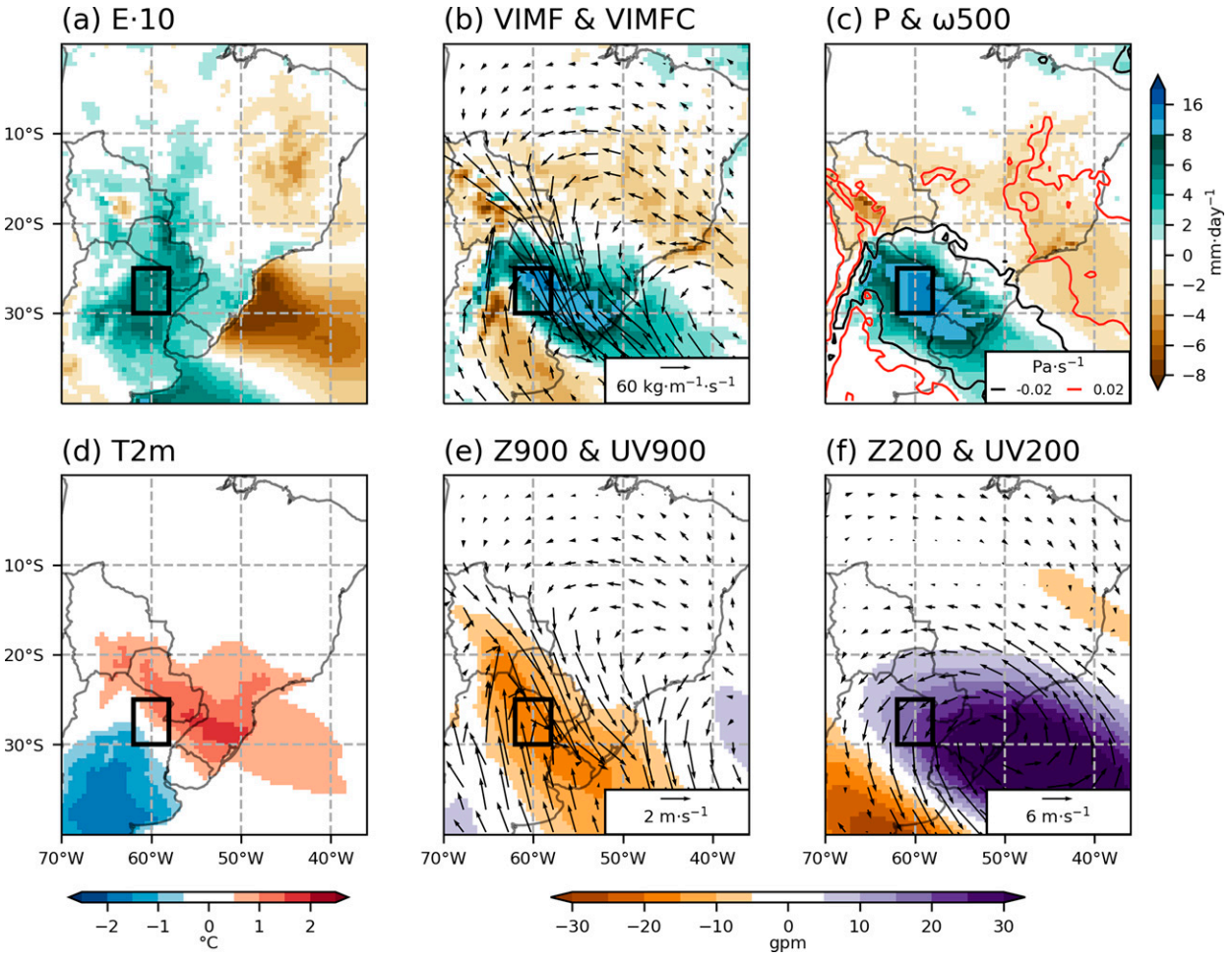

FIG. 4. Monsoon (wet) season 1983–2012 CTL anomalies of the rainy-night days composites with respect to the mean climate (Fig. 2). Only values that are statistically significant at the 95% level according to Welch's *t* test are shown. The outlined rectangle indicates the JEXIT region; *E* is multiplied by 10 to be comparable to the scale of changes in *P* and VIMFC.

We now explore the possible relationships between the *P* event, the atmospheric conditions in its surroundings, and the regional circulation, in CTL. Figure 5 shows the temporal correlations between the time series of the area-averaged *P* in JEXIT and the different variables at each grid point within the whole domain. The time series are composed of daily anomalies with respect to the monthly mean in order to avoid seasonal biases in the results. The rainy-night *P* in JEXIT is positively correlated with the *E* in central-eastern Paraguay (Fig. 5a) and with the northwesterly VIMF and UV900 in Bolivia and western Paraguay (Figs. 5b,e, vectors). There is a high positive relationship with the VIMFC and the upward motion in JEXIT and its surroundings (Figs. 5b,c). Negative correlation values can be observed with T2m to the west of JEXIT in northwestern Argentina (Fig. 5d), consistently with the correlation with the southerly UV900 bringing cold air (Fig. 5e, vectors). At 900 hPa, there is a positive correlation with the geopotential height to the south of JEXIT and a negative correlation from JEXIT itself toward most of Paraguay and Bolivia (Z900 in Fig. 5e). The correlations with T2m, UV900, and Z900 show the relationship between the nocturnal *P* in JEXIT and the cold front intrusion and the intensification of the SALLJ. The correlation with *E* in central-eastern Paraguay, however, does not necessarily imply that the extra *E* over that region directly contributes to the *P* in JEXIT, since the prevailing direction of the flow from that region does not point to JEXIT (Figs. 4b,e). Finally, a correlation with an anticyclonic (cyclonic) anomaly to the southeast (northeast) of JEXIT is observed in the upper troposphere (Fig. 5f), following the anomalies related to the wave train (Fig. 4f).

d. Local and nonlocal land–atmosphere coupling: Effect on the mean climate and JEXIT rainy-night days

We will now explore the changes in the mean climate due to the land–atmosphere coupling by comparing both simulations (CTL and UNC). Figure 6 shows the CTL–UNC climate mean differences of the same variables of Fig. 2. Only statistically significant values are shown. As we mentioned, the comparison

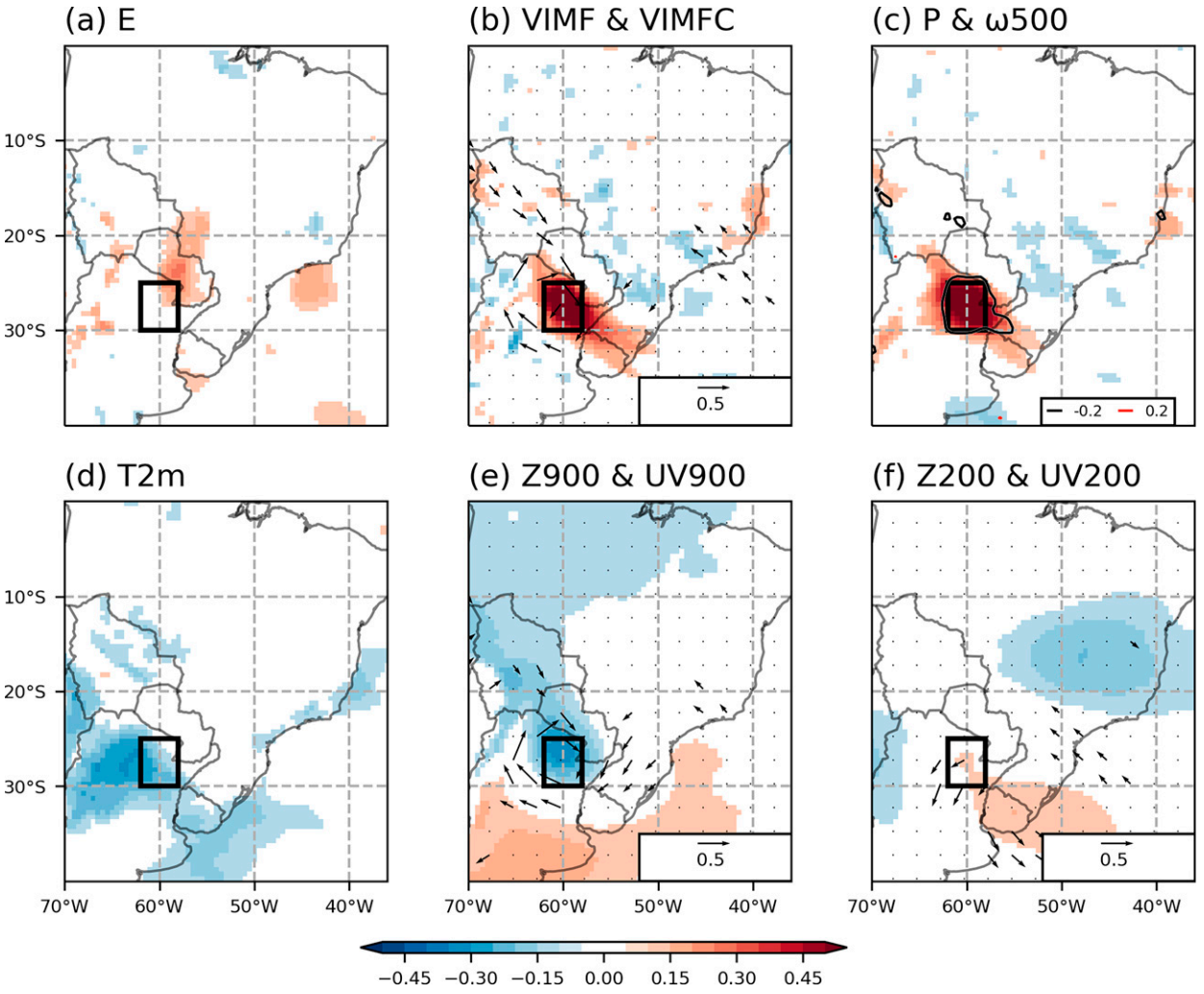

FIG. 5. Daily anomalies temporal correlation between area-averaged P in JEXIT and the same variables of Fig. 2, in each grid point of the domain for JEXIT rainy-night days in CTL during the monsoon (wet) season for 1983–2012. The anomalies are with respect to the monthly mean to avoid seasonal biases. Only values that are statistically significant at the 95% level according to Student's t test are shown. The outlined rectangle indicates the JEXIT region.

between CTL and UNC simulations allows us to isolate the influence that the variability of SM (in particular, its interannual variability) has on the atmosphere, thus areas with maximized absolute differences are the most affected by the land–atmosphere coupling. We observe two areas of higher T2m and lower E in CTL, one located in eastern Brazil and the other one in SESA, mainly central Argentina (Figs. 6a,d; E is multiplied by 5 to be comparable to the scale of changes in P and VIMFC). These two areas correspond with the known SM–atmosphere local coupling hot spots identified by previous works and here with the TCI (Fig. 3).

The coupling also promotes changes in the circulation at low (900 hPa) and high (200 hPa) tropospheric levels and the regional horizontal moisture flux (Figs. 6b,e,f). The geopotential height at 900 hPa gets reduced throughout the domain in CTL, but mainly around the eastern Brazil coupling hot spot (Fig. 6e), which is related to the increase in T2m, thus promoting a thermal low perturbation. Shifts in the form of a cyclonic gyre are observed in UV900 centered around eastern Brazil. Since most of the atmospheric moisture is located at low levels, the CTL-UNC VIMF also shows a cyclonic pattern, although centered around southeastern Brazil. This difference in VIMF mainly opposes the continental-scale anticyclonic gyre (Fig. 2b), especially in SESA. The VIMFC increases in eastern Brazil and gets reduced in the Amazon region, while in SESA there are mixed patches of increased and decreased convergence (Fig. 6b). At 200 hPa we observe an increase in the geopotential height and an anticyclonic pattern in the change in winds, especially in tropical latitudes (Fig. 6f). The P is higher in central-eastern Brazil in CTL (up to approximately a 20% difference) and slightly lower almost everywhere else in the continent (Fig. 6c). The changes in P are consistent with changes in ω500, with greater upward motion in areas with increased P in eastern Brazil (Fig. 6c).

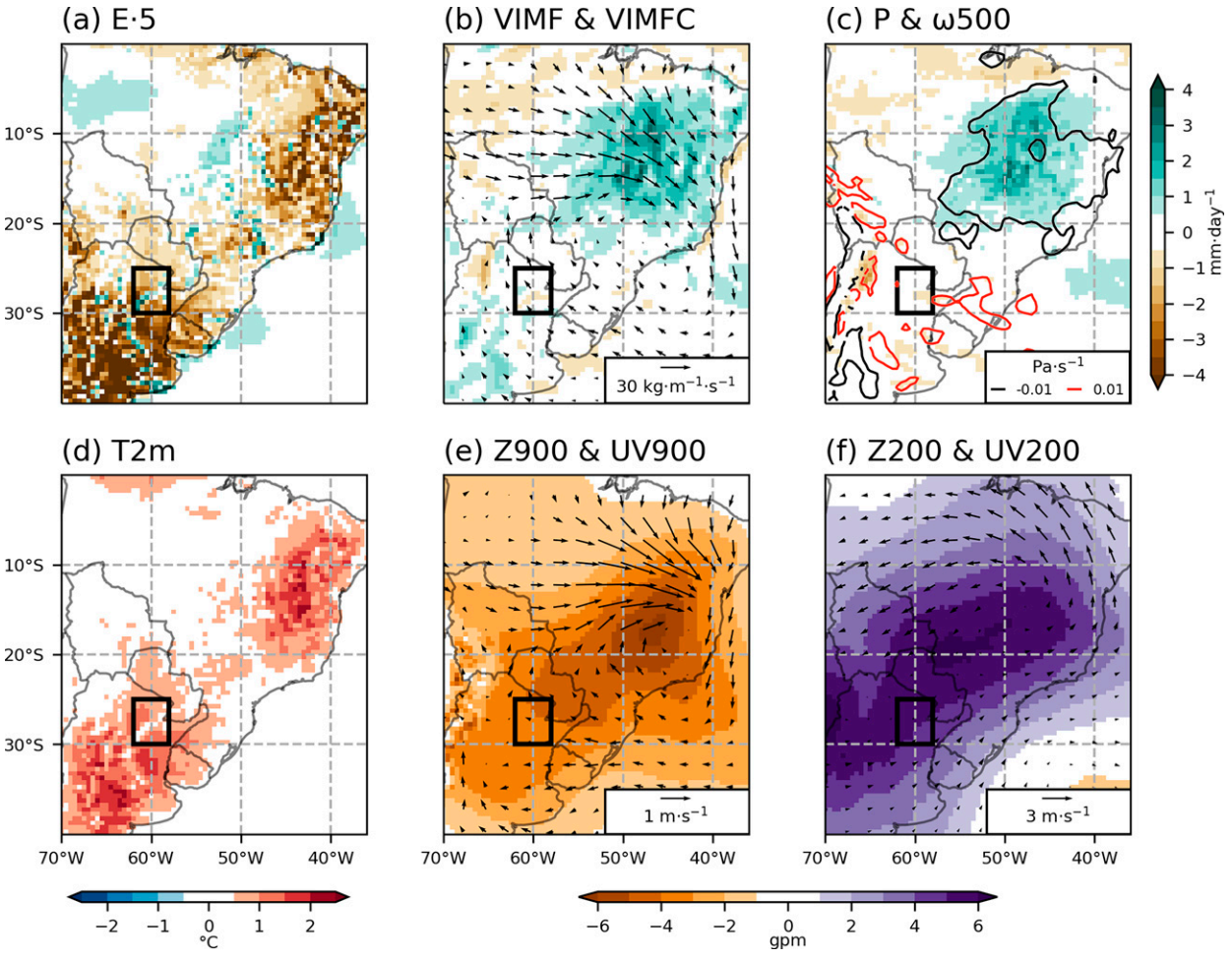

FIG. 6. Changes in the mean climate due to the land–atmosphere coupling, showing monsoon (wet) season 1983–2012 climate mean CTL–UNC differences of the same variables of Fig. 2. Only values that are statistically significant at the 95% level according to Welch's *t* test are shown. The outlined rectangle indicates the JEXIT region; *E* is multiplied by 5 to be comparable to the scale of changes in *P* and VIMFC.

Last, we explore the differences between CTL and UNC for the composites of JEXIT rainy-night days in Fig. 7. In CTL, the higher T2m and lower *E* hot spot located over eastern Brazil is now stronger than the one over SESA (Figs. 7a,d; *E* is multiplied by 5 to be comparable to the scale of changes in *P* and VIMFC), the latter being weaker than in the CTL–UNC climate mean (Figs. 6a,d). This is consistent with the analysis of the TCI (Fig. 3): the local coupling gets weaker around JEXIT during rainy-night days. Nevertheless, there is still a reduction of *E* north of JEXIT in CTL relative to UNC, which is somewhat higher than in the CTL–UNC climate mean. The remaining variables (except for Z200 and UV200 in Fig. 7f) show similar spatial patterns to those in Fig. 6 but with higher intensity in some regions. For example, the anticyclonic shift in VIMF and UV900 is more intense during JEXIT rainy-night days relative to the mean climate (Figs. 6b and 7b), especially along 30°S and the SALLJ region. In other words, the SM (in particular its interannual variability) has a higher impact on the mean regional circulation at low tropospheric levels during JEXIT rainy-night days than in the climate mean.

Changes in geopotential height at 200 hPa show less influence of the coupling in the composition of rainy-night days in comparison with the climate mean (Figs. 6f and 7f). The large-scale dynamical forcing driving these events is possibly overshadowing the influence of the SM. In addition, the absence of significant differences in Z200 is favored by the low variability of the geopotential height at tropical latitudes (Kidson 1999) and by the fact that this atmospheric level is far from the surface. However, cyclonic and anticyclonic gyres are still evident over the southern Atlantic coast and central-eastern Brazil, respectively (UV200 in Fig. 7f). These gyres tend to oppose the anomalous circulation in the upper troposphere related to the occurrence of JEXIT rainy-night days (Fig. 4f), suggesting that the land–atmosphere coupling could slightly weaken the magnitude of these anomalies related to the wave train. Upward motion is observed in eastern Brazil together with increased *P* (Fig. 7c), hinting at increased

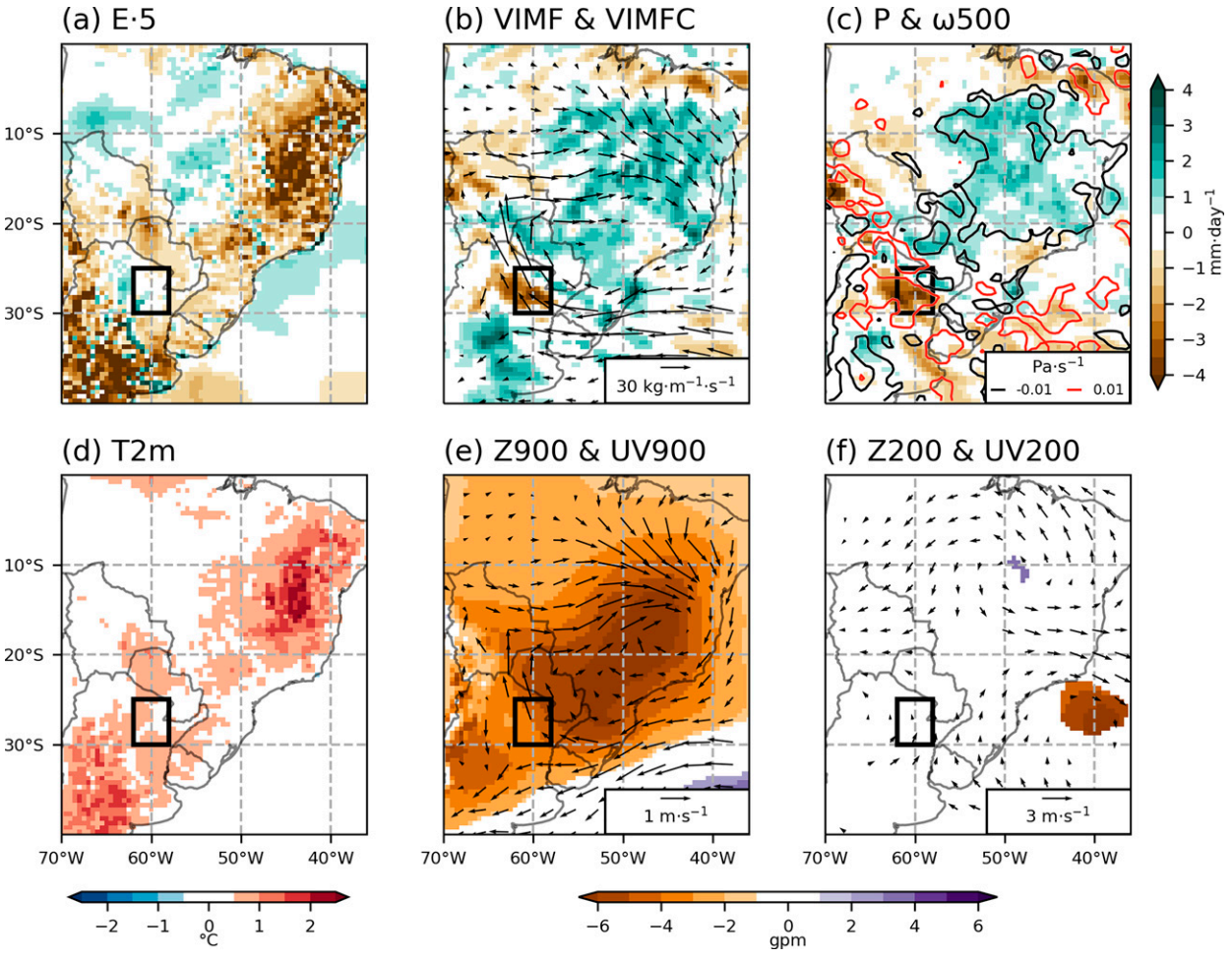

FIG. 7. Changes in the composition of JEXIT rainy-night days due to the land–atmosphere coupling, showing mean monsoon (wet) season 1983–2012 JEXIT rainy-night days CTL-UNC differences of the same variables of Fig. 2. Only values that are statistically significant at the 95% level according to Welch's *t* test are shown. The outlined rectangle indicates the JEXIT region; *E* is multiplied by 5 to be comparable to the scale of changes in *P* and VIMFC.

convection and diabatic warming in this region in CTL, similarly to the analysis of the climate mean; and pronounced compensatory subsidence is evident in JEXIT and other extratropical areas (ω500 in Fig. 7c), inhibiting middle-tropospheric upward motion.

The combination of the aforementioned factors limits the *P* in JEXIT during rainy-night days in CTL, even to a greater extent than in the climate mean. Therefore, the nonlocal effect of the land–atmosphere coupling (only active in CTL) results in reduced *P* in a stripe from northwestern Argentina to Uruguay, covering most of JEXIT (Fig. 7c), in a diagonal spatial pattern following the cold front associated with these rainy events.

Even though the Z900 CTL–UNC difference is negative over central-northern Argentina, Paraguay and southern Bolivia in both the climate mean and the JEXIT rainy-night days composition (Figs. 6e and 7e), which should deepen the Chaco low and thus foster the northerly winds and low-level convergence in JEXIT in CTL relative to UNC, it is not intense enough to counteract the continental-scale gyre related to the perturbation over eastern Brazil. In addition, the *E* in Bolivia and Paraguay contributes to the horizontal moisture flux that finally reaches SESA through the SALLJ (van der Ent et al. 2010; Zemp et al. 2014) and the *E* in that area is reduced in CTL relative to UNC, as a direct consequence of the land–atmosphere coupling but also because of reduced low-level winds. However, the magnitude of these changes in *E* appears small, and we cannot be certain from our analyses that they significantly impact the *P* at JEXIT.

4. Discussion

Two main hot spots of local land–atmosphere coupling were identified, one in SESA and another one in eastern Brazil, where SM variability exerts significant control over *E* and T2m. Both regions have also been recognized as coupling hot spots in previous studies from seasonal to interannual time scales (Sörensson and Menéndez 2011; Wei and Dirmeyer 2012;

Ruscica et al. 2015, 2016; Spennemann et al. 2018; Menéndez et al. 2019). In addition, our study shows that, even if a region (such as JEXIT) has a relatively strong local coupling climatologically, the magnitude of the coupling is dependent on the atmospheric conditions, and it becomes stronger during certain events, such as clear-sky days, or negligible during others, like rainy-night days.

In general, the CTL simulation has lower mean E and higher mean T2m than the UNC one, especially over the two local coupling hot spots in SESA and eastern Brazil. Since both simulations have equal mean SM, this difference must come from the SM variability. In fact, we can confirm this by looking at Fig. 1: in years where the soil in JEXIT is drier than normal, like 2005, the difference in E due to the coupling (CTL vs UNC) is considerably higher than in years when the soil is wetter or has near-average moisture. Thus, in years with drier soils (lower E and higher T2m) the land–atmosphere coupling seems to have a greater impact on the mean climate when compared with wetter years. Ultimately, there is a significant absolute difference of climate mean E (>0.2 mm day^{-1}) between simulations in JEXIT (Fig. 1). This asymmetry is consistent with previous studies that found that the climate variability in La Plata Basin is more sensitive to dry than to wet years (Ruscica et al. 2015; Coronato et al. 2020) and that the coupling promotes warmer and drier conditions (Ma et al. 2011). The results are also consistent with those of Menéndez et al. (2019) for T2m, not only for RCA4 but also in comparison with the LMDZ model: the land–atmosphere coupling affects both the interannual variability and the climate mean of T2m (e.g., their Fig. 5). We also observed other robust changes in the mean values of P and horizontal moisture flux at tropical latitudes and in geopotential heights and winds—at low (900 hPa) but also at upper (200 hPa) tropospheric levels—in tropical and subtropical latitudes. Overall, eastern Brazil and its surroundings stand out as the largest region where the mean state is highly sensitive to the land–atmosphere coupling. Note that the SM variability also affects the circulation over the Atlantic Ocean, even though it was not the focus of our work.

Spatial patterns of different variables obtained from composites and anomalies of JEXIT rainy-night days showed that they are mostly related to Chaco jet–like events (Salio et al. 2002). Moreover, the nocturnal P in JEXIT was found to be correlated with many of the analyzed components of the event, like the deepening of the Chaco low, the intrusion of a cold front and the intensified northerly moisture flux, consistently with previous studies (e.g., Garreaud and Wallace 1998; Garreaud and Aceituno 2007; Mulholland et al. 2018). We confirmed the hypothesis proposed in Giles et al. (2021) that nocturnal P in northeastern Argentina during JEXIT rainy-night days is driven by nonlocal forcings and is not modulated by the local land–atmosphere coupling, despite JEXIT being inside the known SESA hot spot.

Although JEXIT rainy-night days are not correlated with local land–atmosphere coupling, they have less P in the coupled simulation (Giles et al. 2021). Our results suggest that the SM variability over the rest of the continent affects the continental-scale circulation, modulating the P events even in situations with negligible local coupling. We propose a nonlocal coupling mechanism by which the SM variability links the two local coupling hot spots through circulation changes (Fig. 8). The coupling promotes warmer and drier conditions in both hot spots and leads to a thermal low perturbation in eastern Brazil. Low-level (900 hPa) wind convergence and upward motion (500 hPa) are then fostered in eastern Brazil, bringing moisture to the region and promoting more P. A cyclonic (anticyclonic) wind perturbation develops at lower (upper) tropospheric levels. Consequently, two branches of processes get triggered. On the one hand, the cyclonic wind shift at low levels introduces a westerly anomaly in the tropical circulation toward eastern Brazil and slows down the northerly winds in Paraguay and northeastern Argentina, reducing the horizontal moisture flux into subtropical latitudes. On the other hand, compensatory subsidence develops in the middle troposphere (500 hPa) around northeastern Argentina as a consequence of the upward motion in eastern Brazil and the upper-level anticyclone. Then, the combination of decreased moisture flux convergence and inhibited upward motion reduces the total P in parts of SESA like northeastern Argentina (JEXIT), Uruguay and southern Brazil. This nonlocal mechanism is apparent at both the climate mean and the composition of JEXIT rainy-night days.

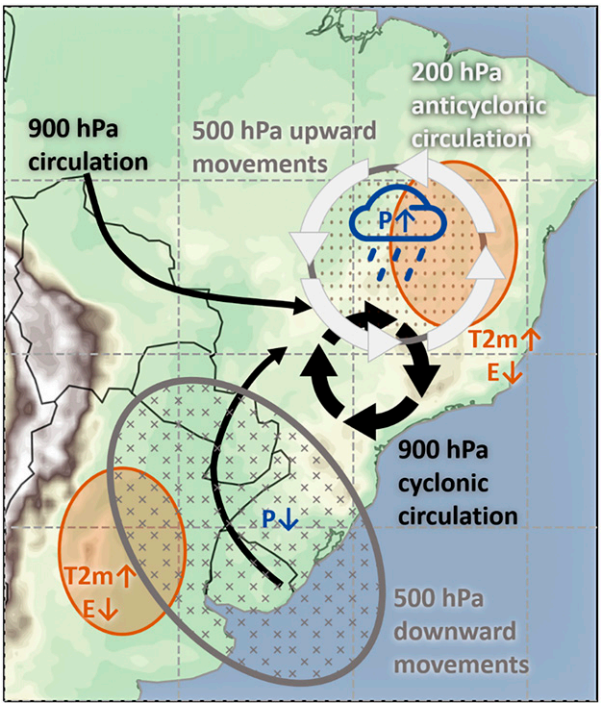

FIG. 8. Schematic illustration of the regional nonlocal coupling mechanism between eastern Brazil and SESA (particularly JEXIT). CTL-UNC differences are pointed out, i.e., the characteristics promoted by the land–atmosphere coupling. Black, gray, and white colors mean changes in the circulation of low, middle, and high tropospheric levels, respectively. Refer to section 4 for a complete description.

However, the analysis of specific events (JEXIT rainy-night days) showed us that the strength of the proposed mechanism depends on the local atmospheric conditions and on how nonlocal sensitivities compare to the local sensitivities, similarly to previous studies (e.g., Wei and Dirmeyer 2019). During rainy-night days in JEXIT the local coupling is absent and the nonlocal forcings are dominant, thus, the nonlocal coupling mechanism becomes more relevant and intense than when considering the climate mean, modulating the regional characteristics of those events. Two components related to JEXIT rainy-night days, the horizontal moisture transport and the vertical motion in the middle troposphere, are modulated by the nonlocal coupling. Even though the Chaco low is deepened in the coupled simulation, which would intensify the northerly low-level winds, the impact of the large cyclonic perturbation centered in eastern Brazil is strong enough to offset that effect, resulting in a southerly wind difference opposed to the mean value, reducing the horizontal moisture flux and convergence in and around JEXIT. In addition, compensatory subsidence limits the upward motion in JEXIT. These changes then lead to less total P in the JEXIT rainy-night days of the coupled simulation.

The proposed nonlocal mechanism, despite not being the dominant forcing of rainy-night days, produces a difference of about 6% in the mean P in JEXIT during these events (Giles et al. 2021), in comparison with the uncoupled simulation. Although the coupled simulation tends to produce less P amount, it has more rainy events (Giles et al. 2021), probably because the land–atmosphere feedback favors the initiation of convection (D'Odorico and Porporato 2004; Findell et al. 2011). Thus, the coupled simulation has more rainy events that, on average, have less amount of P.

The intensity of land–atmosphere coupling varies among different climate models (Koster et al. 2004; Dirmeyer et al. 2006; Williams et al. 2016; Menéndez et al. 2019) and therefore the use of a single model constitutes a limitation in our work that must be considered. Nevertheless, our results are consistent with previous studies that also used a single model (e.g., Grimm et al. 2007; Ruscica et al. 2015; Bieri et al. 2021). Another potential limitation is related to the fact that model biases may be exacerbated in regions with strong land–atmosphere interactions (e.g., a negative rainfall bias, too-dry soils, and a warm bias could be interrelated in SESA; Carril et al. 2012). Maybe in the future, with high-resolution convection-permitting simulations and more realistic land surface models, we will encounter improved coupling results (Prein et al. 2015). Despite these shortcomings, we believe that the results of our study provide valuable insight and build upon the current knowledge of land–atmosphere interactions in South America.

5. Conclusions

In this paper, we explored the local and nonlocal effects of the SM–atmosphere coupling on some characteristic features of the South American climate, with a particular focus on nocturnal P events in northeastern Argentina (what we called the SALLJ exit region or JEXIT). Two 30-yr experimental simulations (1983–2012) carried out with the RCA4 regional climate model over a domain covering all of South America and adjacent oceans were analyzed during the monsoon wet season (October to March). A control simulation with interactive SM (CTL) was compared with a sensitivity simulation in which the SM is prescribed with daily values of the mean annual cycle, thus decoupling the soil state from the atmosphere (UNC). This experimental setup allows us to study causality by isolating the effect that the SM variability (particularly the interannual variability) has on climate.

SM variability may not only alter the climate locally, but also have nonlocal impacts through changes in the regional circulation. The differences in near-surface variables between the two experiments tend to be larger in the areas of higher local coupling, where the CTL simulation produces lower E and higher T2m relative to UNC. In particular, lower surface pressure develops in the eastern Brazilian hot spot, and the location of this hot spot is critical for the regional climatology because it lies roughly in the center of the continental-scale gyre that transports moisture from the tropical Atlantic Ocean to the Amazon basin and then southward toward SESA (where the JEXIT region is located). Consistently, changes in pressure and temperature horizontal gradients between eastern Brazil and Amazonia, between Brazil and the adjacent ocean and around north-central Argentina, alter the continental-scale circulation and promote nonlocal effects of the SM–atmosphere coupling. This favors, when SM–atmosphere coupling is allowed, the moisture flux from the Amazon basin to central and eastern Brazil, increasing moisture convergence and P in that region, and decreasing the moisture flux reaching northern Argentina through the SALLJ. Thus, we proposed a nonlocal coupling mechanism by which the two main local coupling hot spots of South America are linked through changes in the regional circulation, ultimately affecting the P of both regions. This mechanism is found not only at the climate mean but also at specific event compositions (rainy-night days in JEXIT).

The proposed mechanism has similarities to that described by Grimm et al. (2007), which links the spring SM anomalies with the summer P in eastern Brazil. In addition, the two coupling hot spots described are linked by the variability dipole between the South Atlantic convergence zone (SACZ) and SESA, documented at both the intraseasonal (Nogués-Paegle and Mo 1997; Robertson and Mechoso 2000) and interannual scales (Díaz and Vera 2017). This dipole is usually attributed to teleconnections derived from tropical heat sources in the Indian and Pacific Oceans (Díaz and Aceituno 2003; Grimm 2011; Junquas et al. 2012), and our study suggests that the SM could, in turn, modulate the tail of the wave trains arriving to South America through land–atmosphere interactions. Moreover, the present study motivates the raising of new questions that could lead to future research; for example, can SM conditions have impacts beyond this continent? Some topics that could be explored include the impact on stationary waves (Teng et al. 2019), Rossby wave trains arising from the SACZ toward Africa and the Indian Ocean (DeBlander and Shaman 2017), and cyclone formation in SESA and its consequences on the western South Atlantic Ocean storm track (Pal and Eltahir 2003; Falco et al. 2019b).

In our study we go beyond local influences and discuss nonlocal effects to understand changes that cannot be explained solely by the local interactions, particularly with regard to differences in circulation and *P*. Our findings hint at possible relationships that could contribute to improve the predictability studies in the region at seasonal and interannual scales. Furthermore, previous studies suggested opposite hydrological responses to climate change in Brazil and Argentina (dry and wet response, respectively; Ruscica et al. 2016; Zaninelli et al. 2019). Then, the future coevolution of the two land–atmosphere coupling hot spots could modulate the regional climate, in the case of an increase or decrease in the magnitude or extension of the coupling zones.

Acknowledgments. We thank three anonymous reviewers for providing helpful comments on the paper. This study was funded by Fondo para la Investigación Científica y Tecnológica (FONCYT, Grants PICT-2018-02511 and PICT-2015-3097) and Consejo Nacional de Investigaciones Científicas y Técnicas (CONICET, Grant PIP-11220150100402co). We thank Instituto Franco-Argentino para el Estudio del Clima y sus Impactos (IRL 3351 IFAECI) for providing the funds for publishing this work.

Data availability statement. The datasets generated and/or analyzed during the current study are available from the corresponding author on reasonable request.

REFERENCES

Baker, J. C. A., and Coauthors, 2021: An assessment of land–atmosphere interactions over South America using satellites, reanalysis, and two global climate models. *J. Hydrometeor.*, **22**, 905–922, https://doi.org/10.1175/JHM-D-20-0132.1.

Banerjee, O., M. Cicowiez, C. Z. de Lima, and A. R. Rios, 2021: Climate change impacts on agriculture in Latin America and the Caribbean: An application of the Integrated Economic–Environmental Modeling (IEEM) platform. IDB Working Paper Series No IDB-WP 01289, https://doi.org/10.18235/0003794.

Barros, V. R., J. A. Boninsegna, I. A. Camilloni, M. Chidiak, G. O. Magrín, and M. Rusticucci, 2015: Climate change in Argentina: Trends, projections, impacts and adaptation. *Wiley Interdiscip. Rev.: Climate Change*, **6**, 151–169, https://doi.org/10.1002/wcc.316.

Bechtold, P., E. Bazile, F. Guichard, P. Mascart, and E. Richard, 2001: A mass-flux convection scheme for regional and global models. *Quart. J. Roy. Meteor. Soc.*, **127**, 869–886, https://doi.org/10.1002/qj.49712757309.

Bieri, C. A., F. Dominguez, and D. M. Lawrence, 2021: Impacts of large-scale soil moisture anomalies on the hydroclimate of southeastern South America. *J. Hydrometeor.*, **22**, 657–669, https://doi.org/10.1175/JHM-D-20-0116.1.

Blázquez, J., and A. S. Solman, 2020: Multiscale precipitation variability and extremes over South America: Analysis of future changes from a set of CORDEX regional climate model simulations. *Climate Dyn.*, **55**, 2089–2106, https://doi.org/10.1007/s00382-020-05370-8.

Carril, A. F., and Coauthors, 2012: Performance of a multi-RCM ensemble for south eastern South America. *Climate Dyn.*, **39**, 2747–2768, https://doi.org/10.1007/s00382-012-1573-z.

Collazo, S., O. Lhotka, M. Rusticucci, and J. Kyselý, 2018: Capability of the SMHI-RCA4 RCM driven by the ERA-Interim reanalysis to simulate heat waves in Argentina. *Int. J. Climatol.*, **38**, 483–496, https://doi.org/10.1002/joc.5190.

Conil, S., H. Douville, and S. Tyteca, 2007: The relative influence of soil moisture and SST in climate predictability explored within ensembles of AMIP type experiments. *Climate Dyn.*, **28**, 125–145, https://doi.org/10.1007/s00382-006-0172-2.

Coronato, T., and Coauthors, 2020: The impact of soil moisture–atmosphere coupling on daily maximum surface temperatures in southeastern South America. *Climate Dyn.*, **55**, 2543–2556, https://doi.org/10.1007/s00382-020-05399-9.

DeBlander, E., and J. Shaman, 2017: Teleconnection between the South Atlantic convergence zone and the southern Indian Ocean: Implications for tropical cyclone activity. *J. Geophys. Res.*, **122**, 728–740, https://doi.org/10.1002/2016JD025373.

Dee, D. P., and Coauthors, 2011: The ERA-Interim reanalysis: Configuration and performance of the data assimilation system. *Quart. J. Roy. Meteor. Soc.*, **137**, 553–597, https://doi.org/10.1002/qj.828.

Díaz, A., and P. Aceituno, 2003: Atmospheric circulation anomalies during episodes of enhanced and reduced convective cloudiness over Uruguay. *J. Climate*, **16**, 3171–3185, https://doi.org/10.1175/1520-0442(2003)016<3171:ACADEO>2.0.CO;2.

Díaz, L. B., and C. S. Vera, 2017: Austral summer precipitation interannual variability and trends over southeastern South America in CMIP5 models. *Int. J. Climatol.*, **37**, 681–695, https://doi.org/10.1002/joc.5031.

Dirmeyer, P. A., 2011: The terrestrial segment of soil moisture–climate coupling. *Geophys. Res. Lett.*, **38**, L16702, https://doi.org/10.1029/2011GL048268.

——, R. D. Koster, and Z. Guo, 2006: Do global models properly represent the feedback between land and atmosphere? *J. Hydrometeor.*, **7**, 1177–1198, https://doi.org/10.1175/JHM532.1.

D'Odorico, P., and A. Porporato, 2004: Preferential states in soil moisture and climate dynamics. *Proc. Natl. Acad. Sci. USA*, **101**, 8848–8851, https://doi.org/10.1073/pnas.0401428101.

Ek, M. B., and A. A. M. Holtslag, 2004: Influence of soil moisture on boundary layer cloud development. *J. Hydrometeor.*, **5**, 86–99, https://doi.org/10.1175/1525-7541(2004)005<0086:IOSMOB>2.0.CO;2.

Eltahir, E. A. B., and R. L. Bras, 1996: Precipitation recycling. *Rev. Geophys.*, **34**, 367–378, https://doi.org/10.1029/96RG01927.

Falco, M., A. F. Carril, C. G. Menéndez, P. G. Zaninelli, and L. Z. X. Li, 2019a: Assessment of CORDEX simulations over South America: Added value on seasonal climatology and resolution considerations. *Climate Dyn.*, **52**, 4771–4786, https://doi.org/10.1007/s00382-018-4412-z.

——, L. Z. X. Li, C. G. Menéndez, and A. F. Carril, 2019b: The influence of South American regional climate on the simulation of the Southern Hemisphere extratropical circulation. *Climate Dyn.*, **53**, 6469–6488, https://doi.org/10.1007/s00382-019-04940-9.

FAO-UNESCO, 1981: Soil map of the world: Vol. 5, Europe. UNESCO, https://www.fao.org/soils-portal/data-hub/soil-maps-and-databases/faounesco-soil-map-of-the-world/.

Feron, S., and Coauthors, 2019: Observations and projections of heat waves in South America. *Sci. Rep.*, **9**, 8173, https://doi.org/10.1038/s41598-019-44614-4.

Findell, K., P. Gentine, B. Lintner, and C. Kerr, 2011: Probability of afternoon precipitation in eastern United States and Mexico enhanced by high evaporation. *Nat. Geosci.*, **4**, 434–439, https://doi.org/10.1038/ngeo1174.

Fischer, E. M., S. I. Seneviratne, P. L. Vidale, D. Lüthi, and C. Schär, 2007: Soil moisture-atmosphere interactions during the 2003 European summer heat wave. *J. Climate*, **20**, 5081–5099, https://doi.org/10.1175/JCLI4288.1.

Garreaud, R. D., 2000: Cold air incursions over subtropical South America: Mean structure and dynamics. *Mon. Wea. Rev.*, **128**, 2544–2559, https://doi.org/10.1175/1520-0493(2000)128<2544:CAIOSS>2.0.CO;2.

——, and J. M. Wallace, 1998: Summertime incursions of midlatitude air into subtropical and tropical South America. *Mon. Wea. Rev.*, **126**, 2713–2733, https://doi.org/10.1175/1520-0493(1998)126<2713:SIOMAI>2.0.CO;2.

——, and P. Aceituno, 2007: Atmospheric circulation and climatic variability. *The Physical Geography of South America*, T. Veblen, K. Young, and A. Orme, Eds., Vol. I. Oxford University Press, 45–59.

——, M. Vuille, R. Compagnucci, and J. Marengo, 2009: Present-day South American climate. *Palaeogeogr. Palaeoclimatol. Palaeoecol.*, **281**, 180–195, https://doi.org/10.1016/j.palaeo.2007.10.032.

Giles, J. A., R. C. Ruscica, and C. G. Menéndez, 2020: The diurnal cycle of precipitation over South America represented by five gridded datasets. *Int. J. Climatol.*, **40**, 668–686, https://doi.org/10.1002/joc.6229.

——, ——, and ——, 2021: Warm-season precipitation drivers in northeastern Argentina: Diurnal cycle of the atmospheric moisture balance and land–atmosphere coupling. *Int. J. Climatol.*, **41** (Suppl. 1), E768–E778, https://doi.org/10.1002/joc.6724.

Grimm, A. M., 2011: Interannual climate variability in South America: Impacts on seasonal precipitation, extreme events, and possible effects of climate change. *Stochastic Environ. Res. Risk Assess.*, **25**, 537–554, https://doi.org/10.1007/s00477-010-0420-1.

——, and M. T. Zilli, 2009: Interannual variability and seasonal evolution of summer monsoon rainfall in South America. *J. Climate*, **22**, 2257–2275, https://doi.org/10.1175/2008JCLI2345.1.

——, J. S. Pal, and F. Giorgi, 2007: Connection between spring conditions and peak summer monsoon rainfall in South America: Role of soil moisture, surface temperature, and topography in eastern Brazil. *J. Climate*, **20**, 5929–5945, https://doi.org/10.1175/2007JCLI1684.1.

Gutowski, W. J., Jr., and Coauthors, 2016: WCRP COordinated Regional Downscaling EXperiment (CORDEX): A diagnostic MIP for CMIP6. *Geosci. Model Dev.*, **9**, 4087–4095, https://doi.org/10.5194/gmd-9-4087-2016.

Haarsma, R. J., F. Selten, B. van den Huk, W. Hazeleger, and X. L. Wang, 2009: Drier Mediterranean soils due to greenhouse warming bring easterly winds over summertime central Europe. *Geophys. Res. Lett.*, **36**, L04705, https://doi.org/10.1029/2008GL036617.

Hauser, M., R. Orth, and S. I. Seneviratne, 2017: Investigating soil moisture–climate interactions with prescribed soil moisture experiments: An assessment with the Community Earth System Model (version 1.2). *Geosci. Model Dev.*, **10**, 1665–1677, https://doi.org/10.5194/gmd-10-1665-2017.

Hillel, D., 1980: *Fundamentals of Soil Physics*. Academic Press, 413 pp.

Jaeger, E. B., and S. I. Seneviratne, 2011: Impact of soil moisture–atmosphere coupling on European climate extremes and trends in a regional climate model. *Climate Dyn.*, **36**, 1919–1939, https://doi.org/10.1007/s00382-010-0780-8.

Jones, C., U. Willen, A. Ullerstig, and U. Hansson, 2004: The Rossby Centre regional atmospheric climate model part I: Model climatology and performance for the present climate over Europe. *AMBIO*, **33**, 199–210, https://doi.org/10.1579/0044-7447-33.4.199.

Junquas, C., C. Vera, L. Li, and H. Le Treut, 2012: Summer precipitation variability over southeastern South America in a global warming scenario. *Climate Dyn.*, **38**, 1867–1883, https://doi.org/10.1007/s00382-011-1141-y.

Kain, J. S., and J. M. Fritsch, 1990: A one-dimensional entraining/detraining plume model and its application in convective parameterization. *J. Atmos. Sci.*, **47**, 2784–2802, https://doi.org/10.1175/1520-0469(1990)047<2784:AODEPM>2.0.CO;2.

——, and ——, 1993: Convective parameterization for mesoscale models: The Kain–Fritsch scheme. *The Representation of Cumulus Convection in Numerical Models*, *Meteor. Monogr.*, No. 46, Amer. Meteor. Soc., 165–170.

Kanamitsu, M., and K. C. Mo, 2003: Dynamical effect of land surface processes on summer precipitation over the southwestern United States. *J. Climate*, **16**, 496–509, https://doi.org/10.1175/1520-0442(2003)016<0496:DEOLSP>2.0.CO;2.

Kayano, M. T., R. V. Andreoli, R. A. F. de Souza, and S. R. Garcia, 2017: Spatiotemporal variability modes of surface air temperature in South America during the 1951–2010 period: ENSO and non-ENSO components. *Int. J. Climatol.*, **37** (S1), 1–13, https://doi.org/10.1002/joc.4972.

Kidson, J. W., 1999: Principal modes of Southern Hemisphere low-frequency variability obtained from NCEP–NCAR reanalyses. *J. Climate*, **12**, 2808–2830, https://doi.org/10.1175/1520-0442(1999)012<2808:PMOSHL>2.0.CO;2.

Koster, R. D., M. J. Suarez, and M. Heiser, 2000: Variance and predictability of precipitation at seasonal-to-interannual timescales. *J. Hydrometeor.*, **1**, 26–46, https://doi.org/10.1175/1525-7541(2000)001<0026:VAPOPA>2.0.CO;2.

——, and Coauthors, 2004: Regions of strong coupling between soil moisture and precipitation. *Science*, **305**, 1138–1140, https://doi.org/10.1126/science.1100217.

——, Y. Chang, and S. D. Schubert, 2014: A mechanism for land–atmosphere feedback involving planetary wave structures. *J. Climate*, **27**, 9290–9301, https://doi.org/10.1175/JCLI-D-14-00315.1.

——, ——, H. Wang, and S. D. Schubert, 2016: Impacts of local soil moisture anomalies on the atmospheric circulation and on remote surface meteorological fields during boreal summer: A comprehensive analysis over North America. *J. Climate*, **29**, 7345–7364, https://doi.org/10.1175/JCLI-D-16-0192.1.

Krakauer, N. Y., B. I. Cook, and M. J. Puma, 2010: Contribution of soil moisture feedback to hydroclimatic variability. *Hydrol. Earth Syst. Sci.*, **14**, 505–520, https://doi.org/10.5194/hess-14-505-2010.

Lachaud, M. A., B. E. Bravo-Ureta, and C. E. Ludena, 2017: Agricultural productivity in Latin America and the Caribbean in the presence of unobserved heterogeneity and climatic effects. *Climatic Change*, **143**, 445–460, https://doi.org/10.1007/s10584-017-2013-1.

Lavin-Gullon, A., M. Feijoo, S. Solman, J. Fernandez, R. P. da Rocha, and M. L. Bettolli, 2021: Synoptic forcing associated with extreme precipitation events over southeastern South America as depicted by a CORDEX FPS set of

convection-permitting RCMs. *Climate Dyn.*, **56**, 3187–3203, https://doi.org/10.1007/s00382-021-05637-8.

Ma, H.-Y., C. R. Mechoso, Y. Xue, H. Xiao, C.-M. Wu, J.-L. Li, and F. De Sales, 2011: Impact of land surface processes on the South American warm season climate. *Climate Dyn.*, **37**, 187–203, https://doi.org/10.1007/s00382-010-0813-3.

Marengo, J. A., W. R. Soares, C. Saulo, and M. Nicolini, 2004: Climatology of the low-level jet east of the Andes as derived from the NCEP–NCAR reanalyses: Characteristics and temporal variability. *J. Climate*, **17**, 2261–2280, https://doi.org/10.1175/1520-0442(2004)017<2261:COTLJE>2.0.CO;2.

——, and Coauthors, 2012: Recent developments on the South American monsoon system. *Int. J. Climatol.*, **32** (1), 1–21, https://doi.org/10.1002/joc.2254.

Masson, V., J. L. Champeaux, F. Chauvin, C. Meriguet, and R. Lacaze, 2003: A global database of land surface parameters at 1-km resolution for use in meteorological and climate models. *J. Climate*, **16**, 1261–1282, https://doi.org/10.1175/1520-0442(2003)16<1261:AGDOLS>2.0.CO;2.

Menéndez, C. G., P. G. Zaninelli, A. F. Carril, and E. Sánchez, 2016: Hydrological cycle, temperature, and land surface–atmosphere interaction in the La Plata Basin during summer: Response to climate change. *Climate Res.*, **68**, 231–241, https://doi.org/10.3354/cr01373.

——, and Coauthors, 2019: Temperature variability and soil–atmosphere interaction in South America simulated by two regional climate models. *Climate Dyn.*, **53**, 2919–2930, https://doi.org/10.1007/s00382-019-04668-6.

Montini, T. L., C. Jones, and L. M. V. Carvalho, 2019: The South American low-level jet: A new climatology, variability, and changes. *J. Geophys. Res.*, **124**, 1200–1218, https://doi.org/10.1029/2018JD029634.

Mulholland, J. P., S. W. Nesbitt, R. J. Trapp, K. L. Rasmussen, and P. V. Salio, 2018: Convective storm life cycle and environments near the Sierras de Córdoba, Argentina. *Mon. Wea. Rev.*, **146**, 2541–2557, https://doi.org/10.1175/MWR-D-18-0081.1.

Murgida, A. M., M. H. González, and H. Tiessen, 2014: Rainfall trends, land use change and adaptation in the Chaco salteño region of Argentina. *Reg. Environ. Change*, **14**, 1387–1394, https://doi.org/10.1007/s10113-013-0581-9.

Nogués-Paegle, J., and K. C. Mo, 1997: Alternating wet and dry conditions over South America during summer. *Mon. Wea. Rev.*, **125**, 279–291, https://doi.org/10.1175/1520-0493(1997)125<0279:AWADCO>2.0.CO;2.

Pal, J. S., and E. A. B. Eltahir, 2003: A feedback mechanism between soil-moisture distribution and storm tracks. *Quart. J. Roy. Meteor. Soc.*, **129**, 2279–2297, https://doi.org/10.1256/qj.01.201.

Prein, A. F., and Coauthors, 2015: A review on regional convection-permitting climate modeling: Demonstrations, prospects, and challenges. *Rev. Geophys.*, **53**, 323–361, https://doi.org/10.1002/2014RG000475.

Räisänen, P., M. Rummukainen, and J. Räisänen, 2000: Modification of the HIRLAM radiation scheme for use in the Rossby Centre regional atmospheric climate model. University of Helsinki Department of Meteorology Rep. 49, 71 pp.

Rasch, P. J., and J. E. Kristjánsson, 1998: A comparison of the CCM3 model climate using diagnosed and predicted condensate parameterizations. *J. Climate*, **11**, 1587–1614, https://doi.org/10.1175/1520-0442(1998)011<1587:ACOTCM>2.0.CO;2.

Robertson, A. W., and C. R. Mechoso, 2000: Interannual and interdecadal variability of the South Atlantic convergence zone. *Mon. Wea. Rev.*, **128**, 2947–2957, https://doi.org/10.1175/1520-0493(2000)128<2947:IAIVOT>2.0.CO;2.

Romatschke, U., and R. A. Houze, 2010: Extreme summer convection in South America. *J. Climate*, **23**, 3761–3791, https://doi.org/10.1175/2010JCLI3465.1.

Rowntree, P. R., and J. A. Bolton, 1983: Simulation of the atmospheric response to soil moisture anomalies over Europe. *Quart. J. Roy. Meteor. Soc.*, **109**, 501–526, https://doi.org/10.1002/qj.49710946105.

Ruscica, R. C., A. A. Sörensson, and C. G. Menéndez, 2015: Pathways between soil moisture and precipitation in southeastern South America. *Atmos. Sci. Lett.*, **16**, 267–272, https://doi.org/10.1002/asl2.552.

——, C. G. Menéndez, and A. A. Sörensson, 2016: Land surface–atmosphere interaction in future South American climate using a multi-model ensemble. *Atmos. Sci. Lett.*, **17**, 141–147, https://doi.org/10.1002/asl.635.

Salio, P., M. Nicolini, and A. C. Saulo, 2002: Chaco low-level jet events characterization during the austral summer season. *J. Geophys. Res.*, **107**, 4816, https://doi.org/10.1029/2001JD001315.

——, ——, and E. J. Zipser, 2007: Mesoscale convective systems over southeastern South America and their relationship with the South American low-level jet. *Mon. Wea. Rev.*, **135**, 1290–1309, https://doi.org/10.1175/MWR3305.1.

Samuelsson, P., S. Gollvik, C. Jansson, M. Kupiainen, E. Kourzeneva, and W. J. van de Berg, 2015: The surface processes of the Rossby Centre regional atmospheric climate model (RCA4). SMHI Rep. 157, 58 pp., http://www.smhi.se/polopoly_fs/1.89799!/Menu/general/extGroup/attachmentColHold/mainCol1/file/meteorologi_157.pdf.

Sass, B. H., L. Rontu, H. Savijärvi, and P. Räisänen, 1994: HIRLAM-2 Radiation scheme: Documentation and tests. SMHI Doc. SE-60176 and HIRLAM Tech. Rep. 16, 43 pp.

Saulo, C., J. Ruiz, and Y. G. Skabar, 2007: Synergism between the low-level jet and organized convection at its exit region. *Mon. Wea. Rev.*, **135**, 1310–1326, https://doi.org/10.1175/MWR3317.1.

——, L. Ferreira, J. Nogués-Paegle, M. Seluchi, and J. Ruiz, 2010: Land–atmosphere interactions during a northwestern Argentina low event. *Mon. Wea. Rev.*, **138**, 2481–2498, https://doi.org/10.1175/2010MWR3227.1.

Savijärvi, H., 1990: Fast radiation parameterization schemes for mesoscale and short-range forecast models. *J. Appl. Meteor. Climatol.*, **29**, 437–447, https://doi.org/10.1175/1520-0450(1990)029<0437:FRPSFM>2.0.CO;2.

Seneviratne, S. I., D. Lüthi, M. Litschi, and C. Schär, 2006: Land–atmosphere coupling and climate change in Europe. *Nature*, **443**, 205–209, https://doi.org/10.1038/nature05095.

——, T. Corti, E. L. Davin, M. Hirschi, E. B. Jaeger, I. Lehner, and A. J. Teuling, 2010: Investigating soil moisture–climate interactions in a changing climate: A review. *Earth-Sci. Rev.*, **99**, 125–161, https://doi.org/10.1016/j.earsc irev.2010.02.004.

SMHI, 2021: Rossby Centre regional atmospheric model, RCA4. Swedish Meteorological and Hydrological Institute, https://www.smhi.se/en/research/research-departments/climate-research-at-the-rossby-centre/rossby-centre-regional-atmospheric-model-rca4-1.16562.

Solman, S. A., and J. Blázquez, 2019: Multiscale precipitation variability over South America: Analysis of the added value of CORDEX RCM simulations. *Climate Dyn.*, **53**, 1547–1565, https://doi.org/10.1007/s00382-019-04689-1.

Sörensson, A. A., and C. G. Menéndez, 2011: Summer soil–precipitation coupling in South America. *Tellus*, **63A**, 56–68, https://doi.org/10.1111/j.1600-0870.2010.00468.x.

Spennemann, P. C., M. Salvia, R. C. Ruscica, A. A. Sörensson, F. Grings, and H. Karszenbaum, 2018: Land–atmosphere interaction patterns in southeastern South America using satellite products and climate models. *Int. J. Appl. Earth Obs. Geoinf.*, **64**, 96–103, https://doi.org/10.1016/j.jag.2017.08.016.

Tao, C., Y. Zhang, S. Tang, Q. Tang, H.-Y. Ma, S. Xie, and M. Zhang, 2019: Regional moisture budget and land–atmosphere coupling over the U.S. Southern Great Plains inferred from the ARM long-term observations. *J. Geophys. Res.*, **124**, 10 091–10 108, https://doi.org/10.1029/2019JD030585.

Teng, H., G. Branstator, A. B. Tawfik, and P. Callaghan, 2019: Circumglobal response to prescribed soil moisture over North America. *J. Climate*, **32**, 4525–4545, https://doi.org/10.1175/JCLI-D-18-0823.1.

van der Ent, R. J., H. H. G. Savenije, B. Schaefli, and S. C. Steele-Dunne, 2010: Origin and fate of atmospheric moisture over continents. *Water Resour. Res.*, **46**, W09525, https://doi.org/10.1029/2010WR009127.

Vautard, R., and Coauthors, 2007: Summertime European heat and drought waves induced by wintertime Mediterranean rainfall deficit. *Geophys. Res. Lett.*, **34**, L07711, https://doi.org/10.1029/2006GL028001.

Velasco, I., and J. M. Fritsch, 1987: Mesoscale convective complexes in the Americas. *J. Geophys. Res.*, **92**, 9591, https://doi.org/10.1029/JD092iD08p09591.

Wei, J., and P. A. Dirmeyer, 2012: Dissecting soil moisture–precipitation coupling. *Geophys. Res. Lett.*, **39**, L19711, https://doi.org/10.1029/2012GL053038.

——, and ——, 2019: Sensitivity of land precipitation to surface evapotranspiration: A nonlocal perspective based on water vapor transport. *Geophys. Res. Lett.*, **46**, 12 588–12 597, https://doi.org/10.1029/2019GL085613.

Welch, B. L., 1947: The generalization of Student's problem when several different population variances are involved. *Biometrika*, **34**, 28–35, https://doi.org/10.1093/biomet/34.1-2.28.

Williams, I. N., Y. Lu, L. M. Kueppers, W. J. Riley, S. C. Biraud, J. E. Bagley, and M. S. Torn, 2016: Land–atmosphere coupling and climate prediction over the U.S. Southern Great Plains. *J. Geophys. Res.*, **121**, 12 125–12 144, https://doi.org/10.1002/2016JD025223.

Yang, Z., and F. Dominguez, 2019: Investigating land surface effects on the moisture transport over South America with a moisture tagging model. *J. Climate*, **32**, 6627–6644, https://doi.org/10.1175/JCLI-D-18-0700.1.

Zaninelli, P. G., C. G. Menéndez, M. Falco, N. López-Franca, and A. F. Carril, 2019: Future hydroclimatological changes in South America based on an ensemble of regional climate models. *Climate Dyn.*, **52**, 819–830, https://doi.org/10.1007/s00382-018-4225-0.

Zemp, D. C., C.-F. Schleussner, H. M. J. Barbosa, R. J. van der Ent, J. F. Donges, J. Heinke, G. Sampaio, and A. Rammig, 2014: On the importance of cascading moisture recycling in South America. *Atmos. Chem. Phys.*, **14**, 13 337–13 359, https://doi.org/10.5194/acp-14-13337-2014.

Zhang, Y., and S. A. Klein, 2010: Mechanisms affecting the transition from shallow to deep convection over land: Inferences from observations of the diurnal cycle collected at the ARM Southern Great Plains site. *J. Atmos. Sci.*, **67**, 2943–2959, https://doi.org/10.1175/2010JAS3366.1.